In-Vitro Demonstration of Ultra-Reliable, Wireless and Batteryless Implanted Intracranial Sensors Operated on Loci of Exceptional Points

Minye Yang , Zhilu Ye, Nabeel Alsaab, Mohamed Farhat, and Pai-Yen Chen, Senior Member, IEEE

Abstract—Vital signal monitoring, such as pulse, respiration rate, intra-organ and intra-vascular pressure, can provide important information for determination of clinic diagnosis, treatments, and surgical protocols. Nowadays, micromachined bioimplants, equipped with antennas for converting bio-signals to modulated radio transmissions, may allow remote continuous monitoring of patients' vital signs. Yet, current passive biotelemetry techniques usually suffer from poor signal reproducibility and robustness in light of inevitable misalignment between transmitting and receiving antennas. Here, we seek to address this long-existing challenge and to robustly acquire information from a passive wireless intracranial pressure (or brain pressure) sensor by introducing a novel, high-performance biotelemetry system. In spite of variable inductive links, this biotelemetry system may have absolute accuracy by leveraging the uniqueness of loci of exceptional points (EPs) in non-Hermitian radio-frequency (RF) electronic systems with parity-time (PT) symmetry. Our in-vitro experimental demonstration shows that the proposed intracranial (ICP) monitoring system can provide a sub-mmHg resolution in the ICP range of 0-20 mmHg and ultra-robust wireless data acquisition against the misalignment-induced weakening of inductive link. Our results could provide a practical pathway toward reliable, real-time wireless monitoring of ICP, and other vital signals generated by bio-implants and wearables.

Index Terms—Biomedical measurement, biotelemetry and wireless sensing, intracranial pressure (ICP) monitoring, PT-symmetry, wireless vital sign monitoring.

I. INTRODUCTION

HE CAPABILITY to accurately and continuously measure physiological pressure in the human body is important in the clinical practice and medical research [1]–[5]. Although in-vivo pressure measurements have been routinely carried out,

Manuscript received December 31, 2021; revised February 25, 2022; accepted March 29, 2022. Date of publication April 5, 2022; date of current version May 23, 2022. The work of Pai-Yen Chen was supported by NSF under Grant ECCS-1711409. This paper was recommended by Associate Editor S. Carrara. (Corresponding author: Pai-Yen Chen.)

Minye Yang, Zhilu Ye, Nabeel Alsaab, and Pai-Yen Chen are with the Department of Electrical and Computer Engineering, University of Illinois at Chicago, Chicago, IL 60607 USA (e-mail: myang66@uic.edu; zye27@uic.edu; nalsaa4@uic.edu; pychen@uic.edu).

Mohamed Farhat is with the Computer, Electrical, and Mathematical Science and Engineering Division, King Abdullah University of Science and Technology (KAUST), Thuwal 23955, Saudi Arabia (e-mail: mohamed. farhat@kaust.edu.sa).

Color versions of one or more figures in this article are available at https://doi.org/10.1109/TBCAS.2022.3164697.

Digital Object Identifier 10.1109/TBCAS.2022.3164697

which, however, largely hinders their use in continuous, realtime monitoring and poses problems associated with safety, infection, patient comfort, [6]-[11] etc. Wireless and battery-free pressure sensors opened new pathways for efficient management of chronic diseases, such as heart failure (HF) [12], [13], eye disease [14], [15], and brain injury [16]-[18]. Recently, several wireless implantable pressure sensors have been approved by the U.S. Food and Drug Administration (FDA); examples include CardioMEMS HF system for pulmonary artery pressure monitoring [19] and Triggerfish Smart Contact Lens for intraocular pressure measurement [20]. These implantable sensors typically exploit a compact coil antenna to receive radio signals transmitted from a remote reader coil and backscatter them without the need of internal power supply. Hence, the physiological factors that need to be monitored are encoded in the amplitude, phase, and resonant frequency of reflected radio signals. Although wireless sensing principles based on near-field inductive coupling have been invented since 1967 [21], key challenges limiting their practice have not yet been fully addressed, such as the frequency drift due to coil antenna alignment and low sensitivity due to parasitic effects and power losses in human tissues at high frequencies. The discussion about the intracranial pressure (ICP) was firstly arisen by Alexander Monro and George Kellie back to 18th century and reinforced by America neurosurgeon later [22]-[24]. In general, ICP is a comprehensive product created by a compensation among pressures contributed by brain tissue, cerebral blood volume, and cerebrospinal fluid (CSF) inside the skull [25], [26]. ICP is measured in millimeters of mercury (mmHg) and is normally 7-15 [mmHg] at rest for a supine adult. Abnormal ICP is usually caused by traumatic brain injury (TBI), intracranial space occupying lesions, hydrocephalus, idiopathic intracranial hypertension, and intracranial hemorrhage which may result in severe neurological sequelae [27]–[29]. Therefore, a reliable wireless ICP monitoring system would be of immense value for patients suffering from the ICP elevation. Nonetheless, it remains extremely challenging to remotely monitor the ICP using the inductive coupling-based biotelemetry because human skulls are rigid and thus the ICP variation is on a small pressure scale (i.e., 10-15 [mmHg] [30]). Additionally, since the implanted sensor is invisible, misalignment between coil antennas would unavoidably cause unwanted frequency shift, thus affecting the accuracy, reliability, and robustness of the ICP monitoring system. To date, although several different

the majority sensors rely on the wire connection for data transfer,

1932-4545 © 2022 IEEE. Personal use is permitted, but republication/redistribution requires IEEE permission. See https://www.ieee.org/publications/rights/index.html for more information.

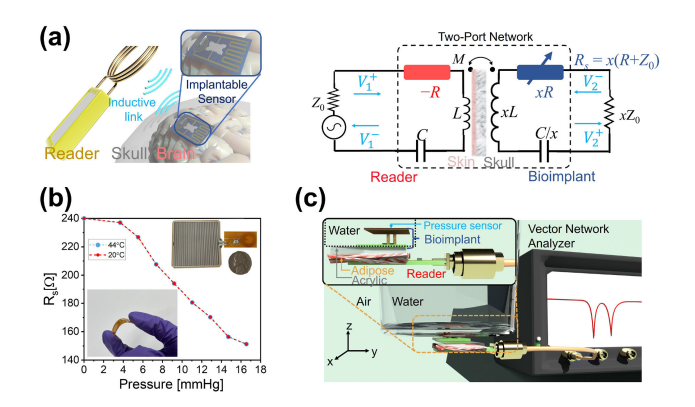


Fig. 1. (a) Schematic and equivalent circuit diagram of the *PTX*-symmetric biotelemetric system used for wireless intracranial pressure (ICP) monitoring. This wireless sensing system has an external reader and a bioimplant, which comprises a pressure-tuned piezoresistive transducer, a micro-coil antenna, and a chip capacitor. (b) Dependency of resistance on the applied pressure for the piezoresistive transducer in two different temperature. The inset of (b) depicts the photograph of wireless ICP sensor. (c) In-vitro experimental setup for wireless ICP monitoring; here, an acrylic board and adipose tissues are placed in between the sensor and reader coils for respectively mimicking human skull and organic tissues.

prototypes (e.g., NEUROVENT-P-tel from RAUMEDIC Inc.) have been demonstrated, the wireless ICP monitoring technique is still facing problems, such as reduction in accuracy compared to those wired methods [9], shortened lifetime due to limited battery durability [31], [32]. Most importantly, inevitable signal drift due to the coil collimation issue becomes more critical for the applications of ICP monitoring since the implanted coil antenna is invisible. In general, passive wireless ICP measurement setups require precise alignment between the coil antenna of the reader and that of the sensor because the system's frequency response is a strong function of its inductive coupling strength [33]. This represents a critical obstacle in clinical practice, as the complicated alignment system not only hinders the mobility of patients, but also brings discomfort. On the other hand, battery enabled wireless ICP monitoring systems [34], [35] may also suffer from mandatory surgeries for maintenance within their short lifetime, which yields increased risk of hemorrhage or inflammatory responses [36]. Besides, the relatively large volume of implanted devices and chemical compositions of batteries are potentially harmful to human organs and tissues.

We herein propose an accurate, continuous biotelemetric technique for wireless and batteryless ICP monitoring by means of tracing loci of exceptional points (EPs) of the non-Hermitian open system with loss and gain. Our method can address the longstanding challenge, i.e., questionary robustness against the coil-antenna misalignment. The system is made of an active reader (-R, L, C) oscillator) and a passive implantable sensor (xR, xL, C/x) oscillator, where x is the scaling factor), as shown in Fig. 1(a). The proposed system is symmetric with respect to the combined parity (P)-time (T)-reciprocal scaling (X) transformation [37]–[40], with its equivalent circuit model shown in Fig. 1(a). By carefully choosing the impedance values of each element in the PTX-symmetric circuit, unidirectional reflectionless properties can be obtained at EPs, which can be seen as spectral singularities in the parameter space of

the system. Besides, EPs can respond sensitively to the perturbations, such as the pressure-adjusted resistance in the ICP sensor (which is equivalent to a variable RLC oscillator [Fig. 1(a)]), thereby enabling high sensitivity and detectability. Moreover, the simultaneous existence of a pair of EPs may allow for compensation of coil misalignment without the need of any sophisticated collimation instrumentation. In the following, we will present theoretical analysis and in-vitro experiment to demonstrate the effectiveness and robustness of the proposed wireless ICP measurement. In our in-vitro demonstrations, a passive wireless ICP sensor comprising a compact coil antenna and an on-chip piezoelectric pressure sensor [Fig. 1(b)], is contactlessly interrogated by an active reader. Here, a composite structure formed by a thick acrylic board and adipose tissues are placed in-between the reader and the sensor, in order to mimic the effect of human skull and skin, as shown in Fig. 1(c). Although this work mainly focuses on real-time ICP monitoring, the proposed telemetry concept can be applied to other wireless implantable biosensor systems for physiological status monitoring.

II. RESULTS AND DISCUSSIONS

A. Theory of PTX-Symmetry Enabled ICP Monitoring

Fig. 1(a) depicts the equivalent circuit model of the PTXsymmetric biotelemetry system comprising inductively coupled oscillators, namely the active reader (-R, L, C resonant tank)and the passive sensor (xR, xL, C/x resonant tank), where the scaling factor x is positive and real. Here, the equivalent resistance of the pressure-tuned piezoresistive transducer R_s = $x(R+Z_0)$ and the reader has a negative resistance element (e.g., negative resistance converter or NRC) connected in series to the radio frequency (RF) signal generator with characteristic impedance Z_0 . This two-port network in Fig. 1(a) is a non-Hermitian electronic system, which follows the *PTX*-symmetry, namely the system is invariant under the combined parity transformation $P(V_1 \leftrightarrow V_2)$, time-reversal transformation $T(t \rightarrow V_2)$ -t), and reciprocal scaling X ($V_1 \rightarrow x^{1/2}V_1, V_2 \rightarrow x^{-1/2}V_2$), where $V_1(V_2)$ corresponds to the voltage across the terminals [39]. Such a system is known to counterintuitively enable exotic physical features, such as EPs where the system experiences phase transitions and coherent perfect absorber-laser (CPAL) points [41]-[47]. The scattering responses of a two-port network can be described using the scattering matrix $\mathbf{S} = \begin{bmatrix} t & r_R \\ r_L & t \end{bmatrix}$, which relates incoming and outgoing voltage signals $(V_1^\pm \text{ and } V_2^\pm)$ as: $(V_1^-, V_2^+)^T = \mathbf{S}(V_1^+, V_2^-)^T$, where r_L , r_R , and t respectively stand for reflection coefficients seen looking into left and right sides of the network and the transmission coefficient (see Appendix A for the explicit expression of S). We should point out that S is independent of the reciprocal scaling factor x. When x=1, the system would degenerate into the PT-symmetric system [48]–[50]. We note that x offers great flexibility in designing the telemetry system. The phase transition in the PTX-symmetric system can be understood from the evolution of eigenvalues of S, $\lambda_{\pm} = (b \pm \sqrt{c_{+}c_{-}})/2a$ [see Appendix A for the expressions of a, b, and c_{\pm}], with the sensor's effective Q factor $\gamma = R^{-1} \sqrt{L/C}$ (i.e., non-Hermiticity in PTX system)

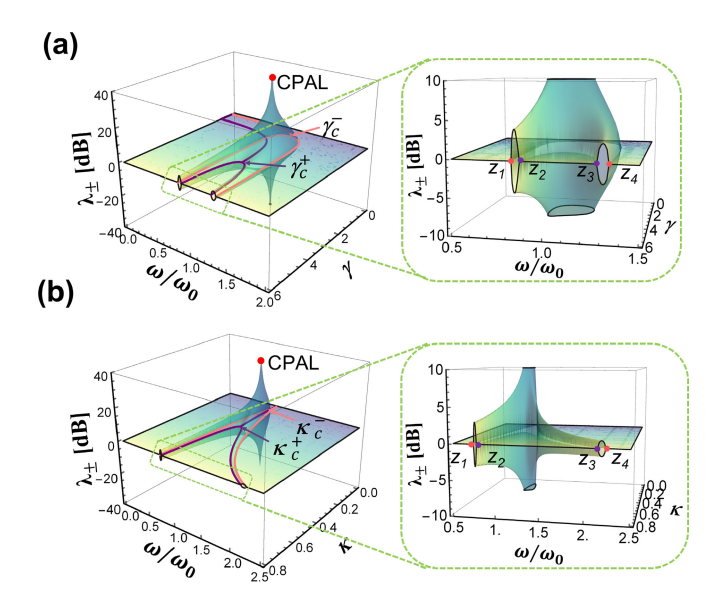


Fig. 2. (a) Contours of eigenvalues as functions of angular frequency ω (in unit of the natural frequency ω_0) and effective Q-factor of the sensor γ for the two-port PTX-symmetric network in Fig. 1(a) under $\kappa=0.45$; here, the ratio of the absolute resistance in the reader to the characteristic impedance of the port $\eta=1.5$. (b) Contours of eigenvalues as functions of ω and κ under $\gamma=4.88$. Magnified views of eigenspectra in (a) and (b) are presented to illustrite exceptional points (zeros in the reflection transfer function); here, (z_2,z_3) and (z_1,z_4) highlighted by colored points correspond to zeros in reflection transfer function $r_L(r_R)$, respectively.

and the coupling coefficient $\kappa = M/\sqrt{L(xL)}$, where $R = \eta Z_0$, M is the mutual inductance between two coil antennas and L is self-inductance of coil antennas. As seen in Figs. 2(a) and (b), when the Q factor γ and the coupling strength κ are varied, the eigenvalues of S experience clear transitions from unimodular ones (exact symmetry phase) to nonunimodular ones (broken symmetry phase) at EPs where the eigenvalues and eigenstates coalesce. There is another type of spectral singularity where zero and infinite eigenvalues would co-exist, as seen in Figs. 2(a) and (b); while $\lambda_{+} = 0$ presents coherent perfect absorption (CPA), $\lambda_{-}=\infty$ results in the lasing effect with bidirectional gigantic reflection [43], [51], [52]. Such a singularity existing in the broken symmetry phase is named as the CPA-laser (CPAL) point. From the circuit analysis perspective, it is convenient to use zeros and poles in unit of the natural frequency of a lossless tank $\omega_0 = 1/\sqrt{LC}$ to describe the EPs and CPAL points, given by:

$$z_{1,2,3,4} = \pm \omega_0 \sqrt{\frac{1 - 2\gamma^2 \xi^2 \pm \sqrt{1 - 4\gamma^2 \xi^2 + 4\kappa^4 \gamma^4 \xi^4}}{2\gamma^2 \xi^2 (\kappa^2 - 1)}};$$
(1a)

$$p_{1,2,3,4} = \omega_0 \frac{-s_{\pm} \pm \sqrt{s_+ - \Delta}}{4},\tag{1b}$$

where $\xi = 1/(1 + \eta^{-1})$ [see Appendix B for explicit expression of poles in (1b)]. From the inset of Figs. 2(a) and (b), we find that the system has four zeros, and among them, z_1 and z_4 correspond to the EPs highlighted by red circles in Figs. 2(a) and

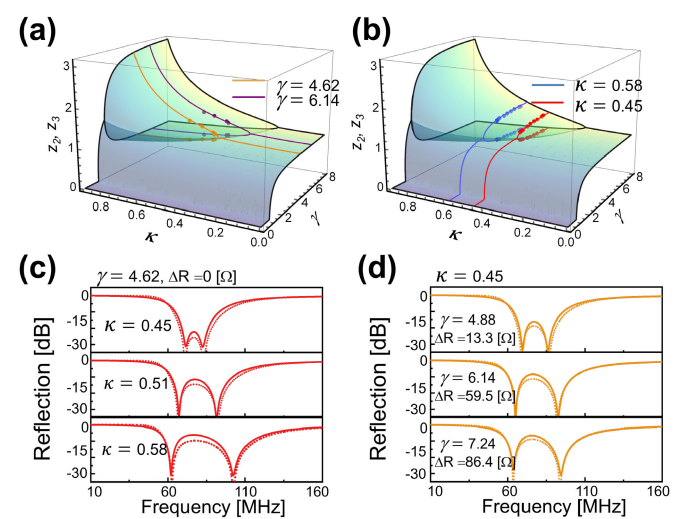


Fig. 3. (a) (b) Loci of exceptional points as a function of γ (a) and κ (b). (c) Measured (solid lines) and calculated (dotted lines) reflection coefficients r_L under different coupling strengths κ , with $\gamma=4.62$; exceptional points or zeros (in unit of $\omega_0=2\pi\times73.12\times10^6\,[{\rm rad/s}]$) obtained from the measurement results are presented in (a). (d) Measured (solid lines) and calculated (dotted lines) reflection coefficient r_L for different values of γ ; here $\kappa=0.45$; zeros obtained from the measurement results are presented in (b).

(b), which result in reflection dips (i.e., $r_R=0$) when an RF generator is connected to the right port. We note that poles, although being of less interest for telemetric sensing due to linearity and stability issues, could be beneficial for design of oscillators and resonators. Figs. 3(a) and (b) present the calculated contours of $z_{2,3}$ as a function of γ and κ with measurement results (dots). It is seen from Figs. 3(a) and (b) that zeros arise after critical points, γ_c^\pm and κ_c^\pm , given by:

$$\gamma_c^{\pm} = \frac{1 \pm \eta^{-1}}{\kappa} \sqrt{\frac{1 \pm \sqrt{1 - \kappa^2}}{2}};$$
 (2a)

$$\kappa_c^{\pm} = \frac{(1 \pm \eta)\sqrt{4\gamma^2\eta^2 - (1 \pm \eta)}}{2\gamma^2\eta^2}.$$
(2b)

We note that under a fixed κ the first (second) kind of unidirectional reflectionless property, $r_L=0$ and $r_R\neq 0$ ($r_L\neq 0$ and $r_R=0$) is obtained when $\gamma>\gamma_c^+$ ($\gamma>\gamma_c^-$). Similarly, under a fixed γ , the first and second kinds of unidirectional reflectionless are obtained when $\kappa > \kappa_c^+$ and $\kappa > \kappa_c^-$, respectively. Hence, the *PTX*-telemetric system can work effectively when γ and κ are higher than the critical values presented in Eqs. (2a) and (2b). More importantly, we know from Eqs. (1) and (2), and Fig. 2 that the unique pair of zeros $(z_{2,3} \text{ and/or } z_{1,4})$ is resulted from a specific set of (γ, κ) . Hence, by tracking the loci of zeros (i.e., resonance frequencies where the dips appear in the reflection spectrum) and applying the values to Eq. (1a), one may be able to retrieve the information of γ related to the sensor information and the inductive coupling strength related to coil alignment and displacement. Since the values of inductance and capacitance of the implantable sensor are pre-known, the pressure information encoded in changes of the resistance can be known $(\gamma = R^{-1}\sqrt{L/C})$. On the contrary, conventional wireless RLC sensor systems [53]–[56] exploiting the passive coil-antenna reader typically exhibit a single weak resonance that depends on both γ and κ . Since different (γ,κ) could result in the same resonant frequency and spectral lineshape, it is therefore difficult to extract the exact value of γ . Such a longstanding issue in passive wireless pressure monitoring system may be addressed by the proposed approach, as it provides an accurate and ultrarobust sensor data acquisition, independent of displacement and alignment between the two coils.

For the circuit shown in Fig. 1(a) with x = 4.8, Figs. 3(c) and (d) plot the calculated (dashed lines) and experimentally measured (solid lines) reflection spectra for the highlighted points in Figs. 3(a) and (b). Here, the reader is connected to a vector network analyzer (VNA; N5242B, Keysight Technologies. Inc) for measuring the scattering parameters. All the lumped components in the circuit are properly selected such that $\kappa > \kappa_c^+$ and $\gamma > \gamma_c^+$ (see Appendix C for details of experimental setups). We find that the evolution of the lineshapes in the reflection spectra (r_L) is varied by γ , with a trend following Eq. (1a), i.e., zeros or resonant reflection dips would rapidly bifurcate around the critical value γ_c^+ . Similar effects are also observed around κ_c^+ , when κ is swept under a fixed γ . Further, there is a good agreement between measurements and theoretical results. Noticeably, under a particular set of condition, there exist two unique zeros in the reflection transfer function r_L , and thus, the exact values of (γ, κ) can be obtained by mapping the measured zeros to contours presented in Fig. 2. As a result, the PTXsymmetric telemetry method may enable accurate and robust data transmission, by means of direct observation of loci of two EPs (zeros), which reflect both the sensor impedance information and the coil alignment condition. In practical short-range biotelemetry, the reader is usually connected to a frequency synthesizer (e.g., VNA with input impedance Z_0), while the passive sensor is terminated by a load resistance (which may be contributed by the sensing or transducing device and thus be variable), as illustrated in Fig. 1(a). To make the above two-port network model valid also in analyzing the system's scattering properties, the equivalent resistance of the sensor is decomposed into two components, $R_s = xR + xZ_0$, where xZ_0 is the scaled input impedance of a "virtual" port assumed here to maintain the *PTX*-symmetry condition [see Fig. 1(a)]. In this setup, the VNA can continuously acquire reflection coefficient r_L , whose spectral response allows us to find poles and zeros, necessary for retrieving the sensors' internal information (γ) and the reader-sensor coupling rate (κ) . For a system initially working near the critical value γ_c^+ , a slight resistive perturbation ΔR introduced by, for example, the bioimplant will break the scaled symmetry between the absolute total resistance in the reader and sensor tank circuits (i.e., $x|-R| \neq R_s - xZ_0$) and thus the unidirectional reflectionless phenomenon disappears. The absolute value of negative resistance on the reader side must be adjusted appropriately to reconfigure the system back to PTXsymmetry, which is determined by observation of two distinct resonant dips (zeros) in the measured reflection spectrum. Once the value of γ is retrieved using Eq. (1a), with the pre-known capacitance of mounted capacitor C/x and self-inductance of coil xL on the sensor, the exact value of sensor resistance can be obtained.

B. In-Vitro Wireless ICP Monitoring

We have conducted an in-vitro experimental demonstration of PTX-symmetric biotelemetry system for continuous, real-time ICP monitoring, with the setup shown schematically in Fig. 1(c). The wireless and batteryless ICP sensor [see the inset of Fig. 1(b)] is composed of a micro-coil antenna with inductance $L_s \approx 1210 [\mathrm{nH}]$ loaded with a capacitor with capacitance $C_s \approx$ 4[pF] (C1005NP01H040C050BA, TDK Corporation) and a piezoelectric transducer (FSR01CE, Ohmite) fabricated using flexible printed circuit board (FPCB) technology. The equivalent resistance of the sensor is $R_s = x(R + Z_0)$, whose dependency on the applied pressure is shown in Fig. 1(b), and x = 4.8. The reader is composed of a spiral coil with inductance $L_r \approx$ 252[nH], an NRC with impedance -R and a chip capacitor with capacitance $C_r \approx 18.8 [pF]$ (CGA2B2C0G1H180J050BD, TDK Corporation), which are in series combination. The reader is connected to the VNA with characteristic impedance $Z_0 =$ $50[\Omega]$. In order to mimic the rise of ICP, the wireless ICP sensor is placed at the bottom of a reservoir filled with different volumes of deionized water [see details in Appendix C]. In addition, an acrylic board and a piece of adipose tissue, respectively mimicking skull and human organ tissues, are placed in between the reader and the sensor. In the initial stage, the resistance of the reader should be tuned to $R_R = -(R + Z_0)$. When the volume of water in the reservoir increases, the external pressure P imposed on the piezoelectric transducer will increase, which in turn reduces its effective resistance by ΔR (i.e., $R_s' = x(R + Z_0) - \Delta R$), with results shown in Fig. 1(b). In order to maintain PTX-symmetry, the equivalent resistance of the NRC on the reader must be adjusted accordingly to: $R_R' = -(R + Z_0 - \Delta R/x)$, achieving a scaled resistance but opposite sign compared to the resistance of the implantable sensor. For simplicity, we assume R=0 and thus the NRC can be removed. By that means, the reader should be mounted with a variable resistor (trimmer; PVG3G500C01R00, Bourns Inc.) with resistance $R_t = \Delta R/x$. Under zero initial pressure (i.e., empty water tank), the sensor resistance $R_s = xZ_0 = 240[\Omega]$ and $\gamma = 4.62$. Here, the wireless ICP monitoring system is carefully designed so that $\gamma > \gamma_c^+$, ensuring that during the in-vitro experiment, two EPs-related reflectionless points can be achieved in the spectrum. During the measurement, the cranial pressure could increase the value of γ and the trimmer must be tuned manually or via programmable controller to detect the EP frequencies that result in the reflectionless property. Fig. 4(a) reports the measured reflection coefficient r_L under applied pressure P = 11[mmHg], which results in a corresponding reduction in sensor's resistance by $\Delta R = 59.5 [\Omega]$ [see Fig. 1(b)]. It is seen from Fig. 4(a) that the resonant lineshape in the reflection spectrum is sensitively determined by the trimmer resistance R_t in the reader, and two reflection dips (i.e., z_2 and z_3) are obtained when $R_t = \Delta R/x = 12.4[\Omega]$ (which makes the PTXsymmetry condition valid). When $R_t < \Delta R/x$ or $R_t > \Delta R/x$,

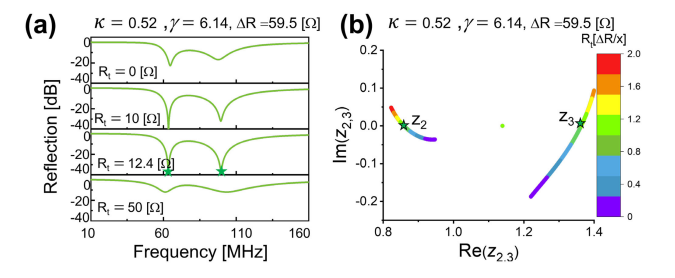


Fig. 4. In-vitro analysis for the *PTX*-symmetric wireless ICP monitoring system. (a) Reflection coefficient r_L versus frequency under pressure $P=11[\mathrm{mmHg}]$ ($R_s=180.5[\Omega]$ or $\Delta R=59.5[\Omega]$), varying the trimmer resistance R_t in the reader. When $R_t\approx \Delta R/x$, two reflection dips emerge as *PTX*-symmetry is obeyed. (b) Evolution of real and imaginary parts of z_2 and z_3 as a function of R_t . Purely real z_2 and z_3 are obtained when $R_t\approx \Delta R/x$.

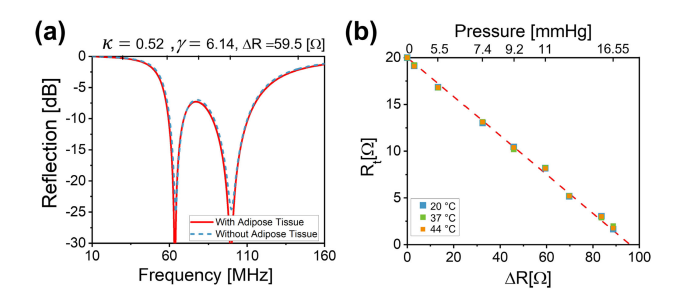


Fig. 5. (a) Experimental measurements of reflection spectra when applied the same pressure with (red solid) and without (blue dashed) adipose tissue and acrylic board placed in-between two coil antennas. (b) ICP measurement under different temperatures.

the resonant disappear due to the destruction of PTX-symmetry. In all measurement, the distance and azimuth between the centers of two coil antennas are fixed to d = (0, 0, 2) [mm]. Once the reflection dips (zeros) are obtained, the value of R_t in the reader can be exploited to deduce the ICP-induced resistance change in the sensor ΔR . Fig. 4(b) presents the loci of real and imaginary parts of zeros under the variation of R_t , under pressure P = 11 [mmHg] $(R_s = 180.5 [\Omega])$. We find that when $R_t = \Delta R/x = 12.4[\Omega]$, two EP-related zeros in the reflection transfer function are purely real, which correspond to reflectionless dips in Fig. 4(a). By applying the measured real zeros in Fig. 4(a) $(z_2, z_3) = (0.86, 1.37)[\omega_0]$ to Eq. (1a), the Q factor and coupling strength can be obtained as: $(\gamma, \kappa) = (6.14, 0.45)$, where $\omega_0 = 2\pi \times 73.12 \times 10^6 [\mathrm{rad/s}]$. Although the measured real zeros could be different for each sensor telemetry (due to the change in the position of the portable reader and the corresponding κ), the retrieved pressure value should be consistent, as will be discussed later.

Moreover, we find that the existence of organ tissues and skull will not affect the sensitivity and resolvability of the proposed ICP monitoring system. Fig. 5(a) compares the measurement results with and without the adipose tissue-acrylic structure under the same applied pressure and the same the coil alignment condition. It can be seen from Fig. 5(a) that the adipose tissues almost have no effect on the measured reflection spectrum, and both resonance frequencies do not shift. This representative example illustrates that this magnetically-coupled wireless ICP monitoring system is reliable even the sensor is embedded in lossy dielectric samples (i.e., biological tissues).

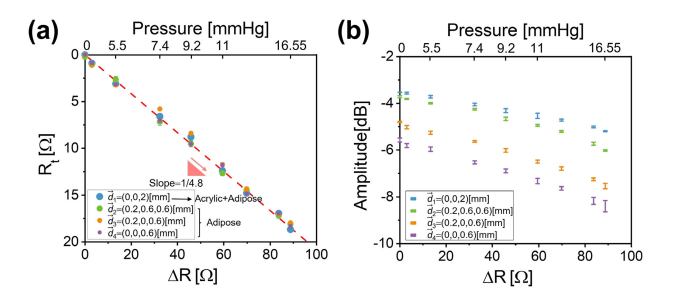


Fig. 6. Comparison of in-vitro experimental results for the PTX-symmetric and traditional biotelemetry methods. (a) Recorded R_t at exceptional points under different applied pressures and in different wireless interrogation scenarios; here, wired measurement was also conducted to measure the resistance change ΔR in the sensor. We note that the R_t versus ΔR curves are almost overlapped, showing a slope of 1/4.8. (b) Amplitude of reflection coefficient versus applied pressure at the resonant frequency $(f_0\approx 76.25 [{\rm MHz}])$ measured using the traditional passive coil antenna; here, the wireless ICP sensor and interrogation scenarios are the same as those used in (a). As usual, the measurement results display discrepancy among different coil alignment conditions.

Fig. 5(b) presents the measurement results obtained at different temperatures, such as the indoor/outdoor room temperature and body temperature. It is seen that the results are insensitive to temperature changes and, thus, the system is suitable for organ pressure/vital signs monitoring. We should also mention that the sensitivity of the proposed ICP monitoring system is determined by the piezoresistive pressure transducer, which, in our design, is $\sim\!6.25[\Omega/\text{mmHg}][\text{see Fig. 1(b)}].$ The sensitivity can be further improved by replacing the commercial pressure transducer with the optimum in-house pressure sensor.

A portable reader ideally offers convenient, continuous and real-time wireless monitoring. However, it is quite difficult to precisely control its position during each interrogation. To illustrate the robustness and reliability of the proposed alignmentand positioning-free biotelemetric technique, Fig. 6(a) presents the measurement results for four different reader-sensor coil positions d_1, d_2, d_3 , and d_4 , which considers both vertical and horizontal coil misalignments. In the first case (d_1) , the two coils are separated by a 1.57 mm-thick acrylic board and a 0.5 mmthick adipose tissue, while for the rest cases $(d_2, d_3, \text{ and } d_4)$, only the adipose tissue is considered. The range of applied pressure is $0 \sim 16.5 [\text{mmHg}]$, which is similar to normal human cranial pressure fluctuations ($10 \sim 15 [mmHg]$). Our experimental results in Fig. 6(a) show that all measured R_t versus ΔR curves have the same slope of 1/x, showing that the proposed telemetry is robust to misalignment and displacement between the reader and the sensor coils. To quantitatively validate the robustness of our system, we set the data point with maximum deviation considering the coil misalignments as:

$$Robustness = \left(1 - \left| \frac{R - R'}{R} \right| \right) \times 100\%, \tag{3}$$

where R is the exact resistance of sensor and R' is deviated resistance of sensor obtained from the measurement. The results reported in Fig. 6(a) shows that the robustness can be 98.17%.

It is also worthwhile mentioning that the scaling factor used in the *PTX*-symmetric system may offer additional design flexibility in selecting transducers with a diverse range of resistance

Publications	TBCAS [31]	JSSC [32]	TBCAS [33]	Nat. Comm. [16]	This Work
Measuring Range (mmHg)	-20-150	0-20	0-40	0-100	0-20
Operating Frequency	416 MHz	-	35 M-2.7 GHz	~5GHz	~100 MHz
Size (mm)	24×19×8	2.2×2.6	10×10	2.5×2.5	20×30
Algorithms	Capacitive change	Capacitive change	Frequency Shift	Frequency Shift	Frequency Shift
Power Supply Method	Battery	Battery	Batteryless	Batteryless	Batteryless
Robust Against Coil Misalignment	-	-	No	No	Yes

TABLE I ICP MONITORING SYSTEMS PERFORMANCE SUMMARY

and sensitivity. A single, multi-purpose reader may be used to interrogate multiple bioimplants in human organs (which have different R, L, and C values to suitably sense different internal organ pressures). For making a comparison, we also use the conventional coil antenna reader [57], [58] to perform the in-vitro experiments in Fig. 6(b), where the pressure-induced resistance variation is monitored based on the amplitude changes at the resonant frequency ($f_0 \approx 76.25 [\text{MHz}]$) [see Appendix D for detailed setups]. Fig. 6(b) reports the measurement results obtained with the conventional near-field measurement method that tracks the resonant frequency shift. It is seen that there exists a large discrepancy in the measured resonance frequencies under different coil alignment conditions. This is because in conventional short-range passive biotelemetry, the resonant frequency shift, modulating the amplitude and/or phase of reflection coefficient, highly depends on the inductive coupling strength [59]. This generally renders misleading data interpretation and questionable reliability. In conventional near-field probing systems, the robustness can be defined by replacing R' and R' in Eq. (3) with the expected resonance frequency f (achieved at d =(0,0,2)[mm]) and the measured second resonance frequency f', respectively. The result shows the robustness is 58.33%, which, when considering the portable reader and the patient's possible mobility, is rather impractical for the wireless ICP measurement. Moreover, we also include a comparison among different current state-of-art of designs of the ICP monitoring systems in Table I. It can be seen that the traditional passive wireless ICP monitoring systems cannot provide such robustness. On the contrary, the proposed PTX-symmetric wireless ICP monitoring system can fundamentally address this issue, thus paving a promising way towards robust, alignment-free passive biotelemetry. We note that although this work focuses on the wireless ICP sensor, similar concept can be readily applied to other implantable sensor, such as intraocular pressure (IOP) sensors and blood pressure sensor. Finally, we note that when implementing our wireless pressure monitoring system to the above applications, biocompatible materials [60] should be used for protecting the physical system and the human body, ensuring a prolonged lifetime.

III. CONCLUSION

We have proposed and conducted the in-vitro study for a new PTX-symmetric biotelemetry system, which may allow for continuous, real-time wireless ICP monitoring. Unlike conventional biotelemetric systems [14], [16], [18], the proposed method does not require complicated alignment and positioning of coil antennas, thus significantly improving the robustness, reliability and convenience. Specifically, the reflection transfer function (i.e., exceptional points) that can be related to the sensor's effective quality factor and the inductive coupling between the sensor and reader coils. We have theoretically proved that the uniqueness found in the loci of exceptional points may guarantee the successful retrieve of the sensor's information and inductive coupling condition. Moreover, the reciprocal scaling operation may offer additional degree of freedom in design of sensors and readers. Our in-vitro experimental results clearly show that the PTX-symmetric wireless ICP monitoring system can have radically improved sensitivity and reliability, particularly for its outstanding tolerance for misaligned coils, when compared with the conventional wireless ICP monitoring [14], [16], [18]. The proposed biotelemetry technique may be beneficial for a wide range of wireless wearables and bioimplants widely used in critical healthcare, vital signs monitoring, and tracking of postoperative recovery.

APPENDIX A

SCATTERING CHARACTERISTICS OF PTX-SYMMETRIC SYSTEM

The scattering matrix S can be obtained using the transfer matrix method [61] as:

$$\mathbf{S} = \begin{bmatrix} t & r_R \\ r_L & t \end{bmatrix} = \frac{1}{a} \begin{bmatrix} b & c_- \\ c_+ & b \end{bmatrix}; \tag{4a}$$

$$a = b + d - 2j\gamma\eta\omega - \omega^2(\eta - 1); \tag{4b}$$

$$b = 2j\gamma\eta\omega^{3}; d = \gamma^{2}\eta^{2}[2\omega^{2} - 1 + (\kappa^{2} - 1)\omega^{4}];$$
 (4c)

$$c_{+} = d - \omega^2(\eta \pm 1). \tag{4d}$$

here, time harmonic notation of $e^{j\omega t}$ is adopted throughout this paper.

APPENDIX B EXPLICIT EXPRESSION OF POLES IN REFLECTION TRANSFER FUNCTION

In this system, poles are solutions of a standard quartic function, given by:

$$p_{1,2,3,4} = \omega_0 \frac{-s_{\pm} \pm \sqrt{s_+^2 - \Delta}}{4}; \tag{5a}$$

$$s_{\pm} = \alpha \pm [\alpha^2 + 4(\mu - (1 - \kappa^2)^{-1})]^{1/2};$$
 (5b)

$$\Delta = 8(\mu s_+ + 2\alpha)/[\alpha^2 + 4(\mu - (1 - \kappa^2)^{-1})]^{1/2};$$
 (5c)

$$\mu = \frac{(-1-j\sqrt{3})[\Theta + (\Theta^2 - P^3)^{1/2}]^{1/3}}{2}$$

$$+\frac{(-1+j\sqrt{3})P}{2[\Theta+(\Theta^2-P^3)^{1/2}]^{1/3}}+\frac{1}{3(1-\kappa^2)}; \hspace{1.5cm} (5d)$$

$$P = \frac{3\alpha^2 + \beta^2 + 12(1 - \kappa^2)^{-1}}{9};$$
 (5e)

$$\Theta = \frac{27\alpha^2 + 9\alpha^2\beta + 2\beta^3 + 27(\alpha^2 - 72\beta)(1 - \kappa^2)^{-1}}{54}; (5f)$$

$$\alpha = j \frac{2}{\gamma \eta(\kappa^2 - 1)}; \beta = \frac{1 - \eta + 2\gamma^2 \eta}{\gamma^2 \eta^2(\kappa^2 - 1)}.$$
 (5g)

APPENDIX C

MEASUREMENT OF PTX-BIOTELEMETRIC SYSTEM

Our PTX-biotelemetric experimental setup consists of a piezoelectric transducer as the bioimplant inductively interrogated by an active reader using the FPCB technology, as shown in Fig. 1(c). The piezoelectric transducer is made of a pressuretuned resistor, loaded with a micro-coil antenna and a chip capacitor. The active reader comprises a -RLC tank mounted with a potential trimmer for adjusting the total resistance of the tank and is connected to the VNA. A piece of acrylic board in thickness of 1.57 [mm] along with a piece of adipose tissue in thickness of 0.5 [mm] are placed in-between two coil antennas for modeling realistic human skull and organ tissues. Two coil antennas are held by micropositioners, which has three degree of freedoms of manipulation, for mimicking the misalignment scenarios in four different relative positions. The piezoelectric transducer is initially placed on the bottom of an empty reservoir corresponding to an ICP of P = 0 [mmHg]. By adding deionized water into the reservoir, the pressure P imposed to the transducer gradually increases, representing the increase of ICP. The monitoring of this pressure, as the vital parameter of interest, is achieved by tracking the loci of EPs from the measured reflection spectrum in the VNA. In the experiment, the pressure range is varied from 0[mmHg] to 16.5[mmHg], covering the normal ICP scale of an adult. Each measured point in Fig. 6(a) is an averaged result from four measurements in total with an error bar applied.

When there is no pressure applied, the sensor coil antenna is designed to be $L_s \approx 1210 [\mathrm{nH}]$ loaded with a chip capacitor with capacitance $C_s \approx 4 [\mathrm{pF}]$ (C1005NP01H040C050BA, TDK Corporation). The reader coil antenna is built to be $L_r \approx$

 $252 [\mathrm{nH}]$, seriesly connected with a chip capacitor with capacitance $C_r \approx 4 [\mathrm{pF}]$ (CGA2B2C0G1H180J050BD, TDK Corporation) and a potential trimmer (PVG3G500C01R00, Bourns Inc.) with the resistance in range of $0 \sim 50 [\Omega]$, which is tuned to be $0 [\Omega]$ initially. Such a circuitry allows the system having an initial Q factor $\gamma = 4.62 > \gamma_c^+$ and x = 4.8. Additionally, since the lumped elements in the system keep unchanged during the ICP monitoring, the resonant frequency of the PTX-symmetric system is $f_0 \approx 73.12 [\mathrm{MHz}]$. The max pressure imposed on the piezoresistive transducer is $16.5 [\mathrm{mmHg}]$, which leads to $\gamma = 7.24$ or $\Delta R = 86.4 [\Omega]$, as shown in Fig. 1(b).

APPENDIX D

MEASUREMENT USING CONVENTIONAL WIRELESS SYSTEM

The ICP monitoring experiment presented by a conventional passive wireless interrogation system makes use of the same piezoresistive transducer. The sensor comprising an RLC oscillator has the same micro-coil antenna being exploited in the PTX-biotelemetric measurement setup, loaded with modified capacitance $C \approx 5[pF]$ (GCQ1555C1H5R1BB01D, Murata Electronics). Whereas the reader of the conventional wireless system is solely made of a micro-coil antenna with an inductance $L \approx 252 [\text{nH}]$ seriesly connected to the VNA, which leads to a signal weak resonance occurring at $f_0 \approx 76.25 [\mathrm{MHz}]$ for closing to the resonant frequency of the PTX-biotelemetric system. The monitoring of the resistive change on the sensor tank reflecting the pressure information is achieved by characterizing the amplitude change at resonant frequency. The variation of pressure is realized in the same way that being exploited in PTX-biotelemetric measurement setup. In addition, to make a fair comparison between these two biotelemetric approaches, we perform the same four relative positions between the centers of two coil antennas as exploited in the PTX-biotelemetric measurement setups to investigate the influence of coil misalignments. As can be seen from Fig. 6, the amplitude change at resonant frequency is significantly altered by the misalignment. Finally, each data point in Fig. 6(b) is also an averaged result from four measurements in total.

REFERENCES

- A. Furniturewalla, M. Chan, J. Sui, K. Ahuja, and M. Javanmard, "Fully integrated wearable impedance cytometry platform on flexible circuit board with online smartphone readout," *Microsyst. Nanoeng.*, vol. 4, no. 1, Dec. 2018, Art. no. 20, doi: 10.1038/s41378-018-0019-0.
- [2] J. Pasek, T. Pasek, K. Sieroń-Stołtny, G. Cieślar, and A. Sieroń, "Electromagnetic fields in medicine the state of art," *Electromagn. Biol. Med.*, vol. 35, no. 2, pp. 1–6, Jul. 2015, doi: 10.3109/15368378.2015.1048549.
- [3] G. Jiang, "Design challenges of implantable pressure monitoring system," Front. Neurosci., vol. 3, 2010, Art. no. 2, doi: 10.3389/neuro.20.002.2010.
- [4] J. O. Lee et al., "A microscale optical implant for continuous in vivo monitoring of intraocular pressure," *Microsyst. Nanoeng.*, vol. 3, no. 1, Dec. 2017, Art. no. 17057, doi: 10.1038/micronano.2017.57.
- [5] A. J. Baneke, J. Aubry, A. C. Viswanathan, and G. T. Plant, "The role of intracranial pressure in glaucoma and therapeutic implications," *Eye*, vol. 34, no. 1, pp. 178–191, 2020.
- [6] J. Shin et al., "Bioresorbable pressure sensors protected with thermally grown silicon dioxide for the monitoring of chronic diseases and healing processes," *Nature Biomed. Eng.*, vol. 3, no. 1, pp. 37–46, Jan. 2019, doi: 10.1038/s41551-018-0300-4.

- [7] W. Lu *et al.*, "Wireless, implantable catheter-type oximeter designed for cardiac oxygen saturation," *Sci. Adv.*, vol. 7, no. 7, Feb. 2021, Art. no. eabe0579, doi: 10.1126/sciadv.abe0579.
- [8] K. Lakhal, S. Ehrmann, and T. Boulain, "Noninvasive BP monitoring in the critically Ill," *Chest*, vol. 153, no. 4, pp. 1023–1039, Apr. 2018, doi: 10.1016/j.chest.2017.10.030.
- [9] U. Kawoos, R. McCarron, C. Auker, and M. Chavko, "Advances in intracranial pressure monitoring and its significance in managing traumatic brain injury," *Int. J. Mol. Sci.*, vol. 16, no. 12, pp. 28979–28997, Dec. 2015, doi: 10.3390/ijms161226146.
- [10] X. Zhang et al., "Invasive and noninvasive means of measuring intracranial pressure: A review," *Physiol. Meas.*, vol. 38, no. 8, 2017, Art. no. R143.
- [11] S. Tavakoli, G. Peitz, W. Ares, S. Hafeez, and R. Grandhi, "Complications of invasive intracranial pressure monitoring devices in neurocritical care," *Neurosurgical Focus*, vol. 43, no. 5, 2017, Art. no. E6.
- [12] Y. S. Choi et al., "Fully implantable and bioresorbable cardiac pacemakers without leads or batteries," *Nature Biotechnol.*, vol. 39, pp. 1228–1238, Jun. 2021, doi: 10.1038/s41587-021-00948-x.
- [13] P. Sharma, X. Hui, J. Zhou, T. B. Conroy, and E. C. Kan, "Wearable radio-frequency sensing of respiratory rate, respiratory volume, and heart rate," *NPJ Digit. Med.*, vol. 3, no. 1, Dec. 2020, Art. no. 98, doi: 10.1038/s41746-020-0307-6.
- [14] J. Kim et al., "A soft and transparent contact lens for the wireless quantitative monitoring of intraocular pressure," Nature Biomed. Eng., vol. 5, no. 7, pp. 772–782, Jul. 2021, doi: 10.1038/s41551-021-00719-8.
- [15] J. Kim et al., "Wearable smart sensor systems integrated on soft contact lenses for wireless ocular diagnostics," *Nature Commun.*, vol. 8, no. 1, Apr. 2017, Art. no. 14997, doi: 10.1038/ncomms14997.
- [16] L. Y. Chen et al., "Continuous wireless pressure monitoring and mapping with ultra-small passive sensors for health monitoring and critical care," *Nature Commun.*, vol. 5, no. 1, Dec. 2014, Art. no. 5028, doi: 10.1038/ncomms6028.
- [17] S.-K. Kang et al., "Bioresorbable silicon electronic sensors for the brain," Nature, vol. 530, no. 7588, pp. 71–76, Feb. 2016, doi: 10.1038/nature16492.
- [18] J. Shin et al., "Bioresorbable optical sensor systems for monitoring of intracranial pressure and temperature," Sci. Adv., vol. 5, no. 7, Jul. 2019, Art. no. eaaw1899, doi: 10.1126/sciadv.aaw1899.
- [19] C. E. Angermann et al., "Pulmonary artery pressure-guided therapy in ambulatory patients with symptomatic heart failure: The CARDIOMEMS E uropean M onitoring S tudy for H eart F ailure (MEMS-HF)," Eur. J. Heart Failure, vol. 22, no. 10, pp. 1891–1901, Oct. 2020, doi: 10.1002/ejhf.1943.
- [20] G. E. Dunbar, B. Shen, and A. Aref, "The sensimed triggerfish contact lens sensor: Efficacy, safety, and patient perspectives," *Clin. Ophthalmol.*, vol. 11, pp. 875–882, May 2017, doi: 10.2147/OPTH.S109708.
- [21] C. C. Collins, "Miniature passive pressure transensor for implanting in the eye," *IEEE Trans. Biomed. Eng.*, vol. BME-14, no. 2, pp. 74–83, Apr. 1967, doi: 10.1109/TBME.1967.4502474.
- [22] A. Monro, "Observations on the structure and functions of the nervous system, illustrated with tables," *London Med. J.*, vol. 4, no. 2, pp. 113–135, 1702
- [23] G. Kellie, "Appearances observed in the dissection of two individuals," Trans. Med. Chirurgical Soc. Edinburgh, vol. 1, no. 1, pp. 84–122, 1824.
- [24] D. S. Nag, S. Sahu, A. Swain, and S. Kant, "Intracranial pressure monitoring: Gold standard and recent innovations," World J. Clin. Cases, vol. 7, no. 13, pp. 1535–1553, Jul. 2019, doi: 10.12998/wjcc.v7.i13.1535.
- [25] L. T. Dunn, "Raised intracranial pressure," J. Neurol., Neurosurg. Psychiatry, vol. 73, no. suppl 1, pp. i23–i27, 2002.
- [26] P. J. Andrews and G. Citerio, "Intracranial pressure," *Intensive Care Med.*, vol. 30, no. 9, pp. 1730–1733, 2004.
- [27] M. Harary, R. G. Dolmans, and W. Gormley, "Intracranial pressure monitoring—Review and avenues for development," *Sensors*, vol. 18, no. 2, Feb. 2018, Art. no. 465, doi: 10.3390/s18020465.
- [28] P. H. Raboel, J. Bartek, M. Andresen, B. M. Bellander, and B. Romner, "Intracranial pressure monitoring: Invasive versus non-invasive Methods—A review," *Crit. Care Res. Pract.*, vol. 2012, pp. 1–14, 2012, doi: 10.1155/2012/950393.
- [29] D. I. Friedman, "Headaches due to low and high intracranial pressure," Continuum: Lifelong Learn. Neurol., vol. 24, no. 4, pp. 1066–1091, 2018.
- [30] M. Czosnyka, "Monitoring and interpretation of intracranial pressure," J. Neurol., Neurosurg. Psychiatry, vol. 75, no. 6, pp. 813–821, Jun. 2004, doi: 10.1136/jnnp.2003.033126.
- [31] H. Jiang, Y. Guo, Z. Wu, C. Zhang, W. Jia, and Z. Wang, "Implantable wireless intracranial pressure monitoring based on air pressure sensing," *IEEE*

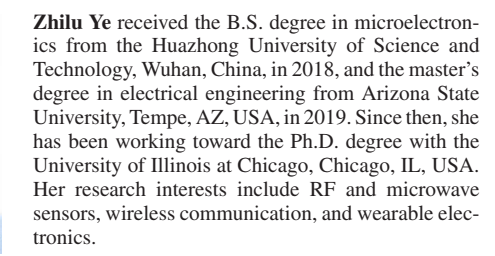
- Trans. Biomed. Circuits Syst., vol. 12, no. 5, pp. 1076–1087, Oct. 2018, doi: 10.1109/TBCAS.2018.2845462.
- [32] M. M. Ghanbari, J. M. Tsai, A. Nirmalathas, R. Muller, and S. Gambini, "An energy-efficient miniaturized intracranial pressure monitoring system," *IEEE J. Solid-State Circuits*, vol. 52, no. 3, pp. 720–734, Mar. 2017, doi: 10.1109/JSSC.2016.2633510.
- [33] F. Wang, X. Zhang, M. Shokoueinejad, B. J. Iskandar, J. E. Medow, and J. G. Webster, "A novel intracranial pressure readout circuit for passive wireless LC sensor," *IEEE Trans. Biomed. Circuits Syst.*, vol. 11, no. 5, pp. 1123–1132, Oct. 2017, doi: 10.1109/TBCAS.2017.2731370.
- [34] A. M. Leung, W. H. Ko, T. M. Spear, and J. A. Bettice, "Intracranial pressure telemetry system using semicustom integrated circuits," *IEEE Trans. Biomed. Eng.*, vol. BME-33, no. 4, pp. 386–395, Apr. 1986, doi: 10.1109/TBME.1986.325794.
- [35] U. Kawoos, M.-R. Tofighi, R. Warty, F. A. Kralick, and A. Rosen, "In-Vitro and in-vivo trans-scalp evaluation of an intracranial pressure implant at 2.4 GHz," IEEE Trans. Microw. Theory Techn., vol. 56, no. 10, pp. 2356–2365, Oct. 2008, doi: 10.1109/TMTT.2008.2004253.
- [36] M. Omidbeigi, M.-S. Mousavi, S. Meknatkhah, M. Edalatfar, A. Bari, and M. Sharif-Alhoseini, "Telemetric intracranial pressure monitoring: A systematic review," *Neurocrit Care*, vol. 34, no. 1, pp. 291–300, Feb. 2021, doi: 10.1007/s12028-020-00992-6.
- [37] Z. Ye, M. Yang, L. Zhu, and P.-Y. Chen, "PTX-Symmetric metasurfaces for sensing applications," *Front. Optoelectron.*, vol. 14, pp. 211–220, Feb. 2021, doi: 10.1007/s12200-021-1204-6.
- [38] Z. Ye, M. Farhat, and P.-Y. Chen, "Tunability and switching of fano and lorentz resonances in PTX-symmetric electronic systems," *Appl. Phys. Lett.*, vol. 117, no. 3, 2020, Art. no. 031101.
- [39] P.-Y. Chen and J. Jung, "P t symmetry and singularity-enhanced sensing based on photoexcited graphene metasurfaces," *Phys. Rev. Appl.*, vol. 5, no. 6, 2016, Art. no. 064018.
- [40] M. Sakhdari, M. Farhat, and P.-Y. Chen, "PT-symmetric metasurfaces: Wave manipulation and sensing using singular points," *New J. Phys.*, vol. 19, no. 6, 2017, Art. no. 065002.
- [41] M. A. K. Othman and F. Capolino, "Theory of exceptional points of degeneracy in uniform coupled waveguides and balance of gain and loss," *IEEE Trans. Antennas Propag.*, vol. 65, no. 10, pp. 5289–5302, Oct. 2017, doi: 10.1109/TAP.2017.2738063.
- [42] C. E. Rüter, K. G. Makris, R. El-Ganainy, D. N. Christodoulides, M. Segev, and D. Kip, "Observation of parity-time symmetry in optics," *Nature Phys.*, vol. 6, no. 3, pp. 192–195, 2010.
- [43] Y. D. Chong, L. Ge, and A. D. Stone, "P t -Symmetry breaking and laser-absorber modes in optical scattering systems," *Phys. Rev. Lett.*, vol. 106, no. 9, Mar. 2011, Art. no. 9, doi: 10.1103/PhysRevLett.106.093902.
- [44] Z. Ye, M. Yang, and P.-Y. Chen, "Multi-band parity-time-symmetric wireless power transfer systems for ISM-band bio-implantable applications," *IEEE J. Electromagn.*, *RF Microw. Med. Biol.*, to be published, doi: 10.1109/JERM.2021.3120621.
- [45] M. Sakhdari, M. Hajizadegan, and P.-Y. Chen, "Robust extended-range wireless power transfer using a higher-order PT-symmetric platform," *Phys. Rev. Res.*, vol. 2, no. 1, Feb. 2020, Art. no. 1, doi: 10.1103/Phys-RevResearch.2.013152.
- [46] M. Sakhdari, M. Hajizadegan, Q. Zhong, D. N. Christodoulides, R. El-Ganainy, and P.-Y. Chen, "Experimental observation of p t symmetry breaking near divergent exceptional points," *Phys. Rev. Lett.*, vol. 123, no. 19, Nov. 2019, Art. no. 19, doi: 10.1103/PhysRevLett.123.193901.
- [47] M. Hajizadegan, M. Sakhdari, S. Liao, and P.-Y. Chen, "High-sensitivity wireless displacement sensing enabled by PT-symmetric telemetry," *IEEE Trans. Antennas Propag.*, vol. 67, no. 5, pp. 3445–3449, May 2019
- [48] M. Farhat, M. Yang, Z. Ye, and P.-Y. Chen, "PT-symmetric absorber-laser enables electromagnetic sensors with unprecedented sensitivity," ACS Photon., vol. 7, no. 8, pp. 2080–2088, Aug. 2020, doi: 10.1021/acsphotonics.0c00514.
- [49] R. El-Ganainy, K. G. Makris, M. Khajavikhan, Z. H. Musslimani, S. Rotter, and D. N. Christodoulides, "Non-Hermitian physics and PT symmetry," *Nature Phys.*, vol. 14, no. 1, Jan. 2018, Art. no. 1, doi: 10.1038/nphys4323.
- [50] M. Yang, Z. Ye, M. Farhat, and P.-Y. Chen, "Ultra-robust wireless interrogation for sensors and transducers: A non-hermitian telemetry technique," *IEEE Trans. Instrum. Meas.*, vol. 70, 2021, Art. no. 1504709, doi: 10.1109/TIM.2021.3107057.
- [51] M. Yang, Z. Ye, M. Farhat, and P.-Y. Chen, "Enhanced radio-frequency sensors based on a self-dual emitter-absorber," *Phys. Rev. Appl.*, vol. 15, no. 1, Jan. 2021, Art. no. 014026, doi: 10.1103/PhysRevApplied.15.014026.

- [52] M. Yang, Z. Ye, M. Farhat, and P.-Y. Chen, "Cascaded PT-symmetric artificial sheets: Multimodal manipulation of self-dual emitter-absorber singularities, and unidirectional and bidirectional reflectionless transparencies," J. Phys. D: Appl. Phys., vol. 55, no. 8, Nov. 2021, Art. no. 085301, doi: 10.1088/1361-6463/ac3300.
- [53] Y. Liang et al., "An LC wireless microfluidic sensor based on low temperature co-fired ceramic (LTCC) technology," Sensors, vol. 19, no. 5, Mar. 2019, Art. no. 1189, doi: 10.3390/s19051189.
- [54] Q. Tan et al., "A LC wireless passive temperature-pressure-humidity (TPH) sensor integrated on LTCC ceramic for harsh monitoring," Sensors Actuators B: Chem., vol. 270, pp. 433–442, Oct. 2018, doi: 10.1016/j.snb.2018.04.094.
- [55] Q. Tan, T. Luo, T. Wei, J. Liu, L. Lin, and J. Xiong, "A wireless passive pressure and temperature sensor via a dual LC resonant circuit in harsh environments," *J. Microelectromech. Syst.*, vol. 26, no. 2, pp. 351–356, Apr. 2017, doi: 10.1109/JMEMS.2016.2642580.
- [56] M. Ma et al., "A novel wireless gas sensor based on LTCC technology," Sensors Actuators B: Chem., vol. 239, pp. 711–717, Feb. 2017, doi: 10.1016/j.snb.2016.08.073.
- [57] R. Nopper, R. Niekrawietz, and L. Reindl, "Wireless readout of passive LC sensors," IEEE Trans. Instrum. Meas., vol. 59, no. 9, pp. 2450–2457, Sep. 2010, doi: 10.1109/TIM.2009.2032966.
- [58] P.-J. Chen, S. Saati, R. Varma, M. S. Humayun, and Y.-C. Tai, "Wireless intraocular pressure sensing using microfabricated minimally invasive flexible-coiled LC sensor implant," *J. Microelectromech. Syst.*, vol. 19, no. 4, pp. 721–734, Aug. 2010, doi: 10.1109/JMEMS.2010.2049825.
- [59] S. Raju, R. Wu, M. Chan, and C. P. Yue, "Modeling of mutual coupling between planar inductors in wireless power applications," *IEEE Trans. Power Electron.*, vol. 29, no. 1, pp. 481–490, Jan. 2014, doi: 10.1109/TPEL.2013.2253334.
- [60] M. Calin et al., "Designing biocompatible Ti-based metallic glasses for implant applications," Mater. Sci. Eng.: C, vol. 33, no. 2, pp. 875–883, 2013
- [61] S. Tretyakov, Analytical Modeling in Applied Electromagnetics. Norwood, MA, USA: Artech House, 2003.



and integrated systems.

Minye Yang received the bachelor's degree in optical and electronic information from the Huazhong University of Science and Technology, Wuhan, China, in 2014, and the M.Sc. degree in electrical and computer engineering from Wayne State University, Detroit, MI, USA, in 2019. He is currently working toward the Ph.D. degree in electrical and computer engineering with the University of Illinois at Chicago, Chicago, IL, USA. His research interests include applied electromagnetics, RF, microwave antennas and circuits, biomedical sensing, metasurfaces, wireless sensors,





Nabeel Alsaab received the first master's degree in electrical engineering from Wayne State University, Detroit, MI, USA, in 2017, and the second master's degree in engineering systems management from St. Mary's University, San Antonio, TX, USA, in 2011. He is currently working toward the Ph.D. degree in electrical engineering with the University of Illinois at Chicago, Chicago, IL, USA. He is currently a Lecturer with the Department of Electrical Engineering, College of Engineering, Qassim University, Unaizah, Saudi Arabia. His extensive programming and project

management skills are applied to the design of smart sensors and wireless communication.



Mohamed Farhat received the master's degree in theoretical physics and the Ph.D. degree in optics and electromagnetism from Aix-Marseille University, Marseille, France. His Ph.D. dissertation was entitled Metamaterials for Harmonic and Biharmonic Cloaking and Superlensing.

He is currently a Research Scientist with the King Abdullah University of Science and Technology, Thuwal, Saudi Arabia. He has authored more than 170 publications, including one edited book, 85 journal articles, seven book chapters, five international

patents, as of August 2021. He has also co-edited the book *Transformation Wave Physics: Electromagnetics, Elastodynamics, and Thermodynamics* (Pan Stanford Publishing). His research interests include the fields of plasmonics and metamaterials with applications spanning optics and acoustics waves.

Dr. Farhat has organized several special sessions at META conferences and is an active reviewer for many international journals in physics, including *Physical Review Letters* and *Nature Physics*.



Pai-Yen Chen (Senior Member, IEEE) received the B.S. and M.S. degrees from National Chiao Tung University, Hsinchu, Taiwan, in 2006 and 2004, respectively, and the Ph.D. degree from the University of Texas at Austin, Austin, TX, USA, in 2013. He is currently an Associate Professor with the Department of Electrical and Computer Engineering, University of Illinois at Chicago, Chicago, IL, USA. He was a Research Scientist with Intellectual Ventures' Metamaterial Commercialization Center during 2013–2014, and a Research Staff with National Nano Device Lab-

oratory, Taiwan, during 2006-2009. He has been involved in multidisciplinary research on applied electromagnetics, RF/microwave antennas and circuits, wireless micro/nano-sensors and integrated systems, nanodevices, and also nanoelectromagnetism in plasmonics and nanophotonics. He was the recipient of quite a few prestigious awards, including the National Science Foundation (NSF) CAREER Award, IEEE Sensors Council Young Professional Award, IEEE Raj Mittra Travel Grant (RMTG) Award, SPIE Rising Researcher Award, ACES Early Career Award, PIERS Young Professional Award, IOP Measurement Science and Technology Emerging Leader, Young Scientist Awards from URSI General Assembly and URSI Commission B: Electromagnetics, Air Force Research Laboratory Faculty Fellowship, National Argonne Laboratory Director's Fellowship, College of Engineering Faculty Research Excellence Award, Donald Harrington Fellowship, Taiwan Ministry of Education Study Abroad Award, United Microelectronics Corporation Scholarship, and quite a few student paper awards and travel grants from main IEEE conferences, including the USNC-URSI Ernest K. Smith Student Paper Award. He is on Board of Directors of Applied Computational Electromagnetics Society (ACES) during 2021-2024. He is currently an Associate Editor for IEEE SENSORS JOURNAL, IEEE TRANSACTIONS ON ANTENNAS AND PROPAGATION, IEEE JOUR-NAL OF RADIO FREQUENCY IDENTIFICATION (IEEE JRFID), IEEE JOURNAL OF ELECTROMAGNETICS, RF AND MICROWAVES IN MEDICINE AND BIOLOGY (IEEE-JERM), and guest editor of several international journals. He was a former Associate Editor for Applied Electromagnetics.